eXPRESS Polymer Letters Vol.2, No.7 (2008) 502–510
Available online at www.expresspolymlett.com
DOI: 10.3144/expresspolymlett.2008.60

Starch-based nanocomposites reinforced with flax cellulose nanocrystals

X. Cao[1], *Y. Chen*[1,2], *P. R. Chang*[1,3*], *A. D. Muir*[1], *G. Falk*[1]

[1]BioProducts and Bioprocesses National Science Program, Agriculture and Agri-Food Canada, 107 Science Place, Saskatoon, SK, S7N 0X2, Canada
[2]Research Centre for Medical and Structural Biology, School of Basic Medical Science, Wuhan University, Wuhan 430071, China
[3]Department of Agricultural and Bioresourse Engineering, University of Saskatchewan, Saskatoon, SK, S7N 5A9, Canada

Received 3 April 2008; accepted in revised form 23 May 2008

Abstract. In this study, the cellulose crystals, prepared by acid hydrolysis of flax fiber, consisted of slender rods with lengths ranging from 100 to 500 nm and diameters ranging from 10 to 30 nm, respectively. After mixing the suspension of flax cellulose nanocrystals (FCNs) and plasticized starch (PS), the nanocomposite films were obtained by the casting method. The effects of FCNs loading on the morphology, thermal behaviour, mechanical properties and water sensitivity of the films were investigated by means of wide-angle X-ray diffraction, differential scanning calorimetry, tensile testing, and water absorption testing. Scanning electron microscopy photographs of the failure surfaces clearly demonstrated a homogeneous dispersion of FCNs within the PS matrix and strong interfacial adherence between matrix and fillers, which led to an increase of glass transition temperature ascribed to the starch molecular chains in the starch-rich phase. In particular, these nanocomposite films exhibited a significant increase in tensile strength and Young's modulus from 3.9 to 11.9 MPa and from 31.9 to 498.2 MPa, respectively, with increasing FCNs content from 0 to 30 wt%. Also, with a loading of FCNs, the resulting nanocomposite films showed a higher water resistance. Therefore, FCNs played an important role in improving the mechanical properties and water resistance of the starch-based materials.

Keywords: *nanocomposites, reinforcements, starch, flax, mechanical properties*

1. Introduction

The development of commodities derived from petrochemical polymers has brought many benefits to mankind. However, it is becoming more evident that the ecosystem is considerably disturbed and damaged as a result of the non-degradable plastic materials used in disposable items. Therefore, the interest in polymers from renewable resources has recently gained exponential momentum and the use of biodegradable and renewable materials to replace conventional petroleum plastics for disposable applications is becoming popular [1, 2]. Within the broad family of renewable polymers, starch is one of the most attractive and promising sources for biodegradable plastics because of the abundant supply, low cost, renewability, biodegradability, and ease of chemical modifications [3, 4]. In recent years, plasticized starch (PS) has attracted considerable attention and has offered an interesting alternative for synthetic polymers where long-term durability is not needed and rapid degradation is an advantage [5]. However, compared with conventional synthetic thermoplastics, biodegradable products based on starch, unfortunately, still exhibit many disadvantages, such as water sensitivity, brittleness, and poor mechanical properties [6]. Vari-

*Corresponding author, e-mail: Changp@agr.gc.ca
© BME-PT and GTE

ous physical or chemical means have been used to solve these problems, including blending with other synthetic polymers [7–9], the chemical modification [10–12], graft copolymerisation [13], and incorporating fillers such as lignin [14], clay [15], and multi-walled carbon nanotubes [16].

More recently, there is an increased use of cellulose nanocrystals (CNs) as the loading-bearing constituent in developing new and inexpensive biodegradable materials due to a high aspect ratio, a high bending strength of about 10 GPa, and a high Young's modulus of approximately 150 GPa [17]. The CNs from various sources such as cotton, tunicate, algae, bacteria, ramie, and wood for preparation of high performance composite materials have been investigated extensively [18]. Both natural and synthetic polymers were explored as the matrixes. Natural polymers such as poly(β-hydroxyoctanoate) (PHO) [19], soy protein [20], silk fibroin [21] reinforced with cellulose whiskers were reported. Meanwhile, Poly-(styrene-*co*-butyl acrylate) (poly(S-*co*-BuA)) [22], poly(vinyl chloride) (PVC) [23], polypropylene [24], waterborne polyurethane [25], were also used as synthetic matrixes.

The flax plant (*Linum usitatissimum*) is a member of the Linaceae family, which is an important crop in many regions of the world. Fibers from flax have been used for thousands of years to make different textile products because of their excellent fiber characteristics. Therefore, the search on short fibers from flax as a replacement for synthetic fibers in many non-textile products, e.g. in polymer compounds, building materials and absorbent materials, has attracted much attention in the last decade [26]. However, incorporating flax cellulose nanocrystals (FCNs) in the starch-based composite films has not been reported in the literatures. In present work, we attempt to prepare CNs from flax fiber by acid hydrolysis with concentrated sulfuric acid, and then use the resulting CNs to reinforce PS for preparation of nanocomposite films with improved performances. The resulting films were prepared by casting the mixture of aqueous suspensions of CNs and PS in various weight ratios. The morphology, structure, and performance of the resulting nanocomposite films were investigated by scanning electron microscopy (SEM), wide-angle X-ray diffraction (WAXD), differential scanning calorimetry (DSC), and measurement of the mechanical properties and water uptake.

2. Experimental

2.1. Materials

Field pea starch, with average granule size of about 29 μm and composed of 35% amylose and 65% amylopectin, was supplied by Nutri-Pea Limited Canada (Portage la Prairie, Canada). Raw flax fiber was supplied by Biolin Research Incorporated, Canada. The glycerol (99% purity), sodium hypochlorite solution (available chlorine 10–13%), sodium hydroxide, and sulfuric acid (98%) were bought from Sigma-Aldrich Canada Ltd. (Oakville, Canada) and used as received.

2.2. Preparation of FCNs

A colloidal suspension of cellulose nanocrystals in water was prepared by acid-catalyzed hydrolysis of flax fiber. Briefly, the flax fiber (30 g) was first cut into small fragments and mixed with sulfuric acid aqueous solution (250 ml, 64%) and stirred vigorously at 45°C for 4 h. Subsequently, the suspension was neutralized with sodium hydroxide aqueous solution (40%), discolored by sodium hypochlorite solution and washed by dialyzing. The dispersion of flax cellulose nanocrystals (FCNs) with a solid content of 1.4 wt% was obtained through a 30 min ultrasonic treatment. The suspension did not sediment or flocculate as a consequence of the surface sulfate groups that were created during the sulfuric treatment [27].

2.3. Preparation of the PS/FCNs nanocomposite films

The fabrication of plasticized starch/flax cellulose nanocrystals (PS/FCNs) composite films was based on a convenient casting solution process. Starch, glycerol, cellulose nanocrystallites suspension and distilled water were mixed together in order to obtain nanocomposite films with a homogeneous dispersion. The glycerol content was fixed at 36 wt% based on the dry starch matrix. Then this mixture was charged into a bottom flask equipped with a stirrer and heated at 100°C for 30 min for the starch to be gelatinized. After cooling down to

about 70°C, the resulting paste was degassed under vacuum to remove the remaining air and cast in a polystyrene square Petri dish, followed by drying in a vent oven at 50°C. By changing the content of FCNs over a range of 5, 10, 15, 20, 25, and 30 wt%, a series of plasticized PS/FCNs nanocomposite films with a thickness of about 0.3 mm were prepared and coded as PS/FCNs-5, PS/FCNs-10, PS/FCNs-15, PS/FCNs-20, PS/FCNs-25, and PS/FCNs-30, respectively, in which the FCNs content was expressed on water-free PS matrix. As a control, a neat PS film without addition of FCNs was obtained using the same fabrication process. Before various characterizations, the resulting films were kept in a conditioning desiccator of 43% relative humidity (*RH*) for one week at room temperature to ensure the equilibration of the water content in the films.

2.4. Characterizations

AFM was used to characterize the morphology of FCNs. Measurements were conducted in tapping mode by a Nanoman AFM (Veeco Metrology Group, USA) at ambient temperature. In the sample preparation, a droplet of dilute FCNs suspension was coated on a flake of mica, and the water was evaporated at ambient temperature.

Scanning electron microscopy (SEM) measurements were carried out on a field-emission scanning electron microscope (FESEM, JEOL JSM-6700, JEOL Ltd, Japan). To study the structure of the nanocomposites, the failure surfaces of the PS/FCNs films after tensile testing was observed. The samples were coated with Platinum and observed with an accelerating voltage of 5 kV.

Attenuated Total Reflectance Fourier Transform Infrared (ATR-FTIR) spectra of the film samples were recorded on a Nicolet 5700 FTIR spectrometer (Thermo Electron Corporation, Waltham, MA, USA). The PS, PS/FCNs-10, PS/FCNs-20 and PS/FCNs-30 films were taken at random from the flat films and data were collected at room temperature over 16 scans with a resolution of 4 cm^{-1}.

Wide-angle X-ray diffraction patterns were recorded on a Bruker AXS X-ray diffraction (Bruker AXS Inc., Madison, WI, USA), using CuK_α radiation (λ = 0.154 nm) at 40 kV and 30 mA with a scan rate of 4°/min. The diffraction angle ranged from 4 to 40°.

Differential scanning calorimetry (DSC) measurement of the films was carried out on a DSC204 apparatus (Netzsch Co., Germany) under a nitrogen atmosphere. Each sample conditioned at 43% *RH* was subjected to the heating/cooling cycle between –100 to 120°C to obtain reproducible glass transition temperature (T_g) values. In this case, T_g was taken at the half-variation in the heat capacity of the second run. The heating rate was 10°C/min.

The tensile strength and elongation at break of the films were measured on a universal testing machine (CMT 6503, Shenzhen SANS Test Machine Co. Ltd., China) at room temperature with gauge length of 5 cm and crosshead speed of 10 mm/min. An average value of five replicates for each sample was taken.

The kinetics of water absorption was determined for all composites. The samples used were thin rectangular strips with dimensions of 50 mm×10 mm× 0.3 mm. The samples were dried at 80°C under vacuum overnight and kept at 0% *RH* (P_2O_5) for one week. After weighing, they were conditioned at room temperature in a desiccator of 98% *RH* ($CuSO_4 \cdot 5H_2O$ saturated solution). The conditioning of samples in high moisture atmosphere was preferred to the classical technique of immersion in water, because starch is very sensitive to water and can partially dissolve after long time exposure to water. The samples were removed at specific intervals and weighed until the equilibrium state was reached. The water uptake (*WU*) of the samples was calculated by Equation (1):

$$WU\,[\%] = \frac{W_t - W_0}{W_0} \cdot 100 \tag{1}$$

where W_0 and W_t were the weights of the sample before exposure to 98% *RH* and after *t* h exposure to 98% *RH*, respectively. An average value of three replicates for each sample was taken.

3. Results and discussions

3.1. Morphology of FCNs and PS/FCNs nanocomposites

The AFM image of a dilute suspension of FCNs in Figure 1 shows that the suspension contains flax cellulose fragments consisting of both individual and aggregated nanocrystals. These fragments display slender rods and have a broad distribution in

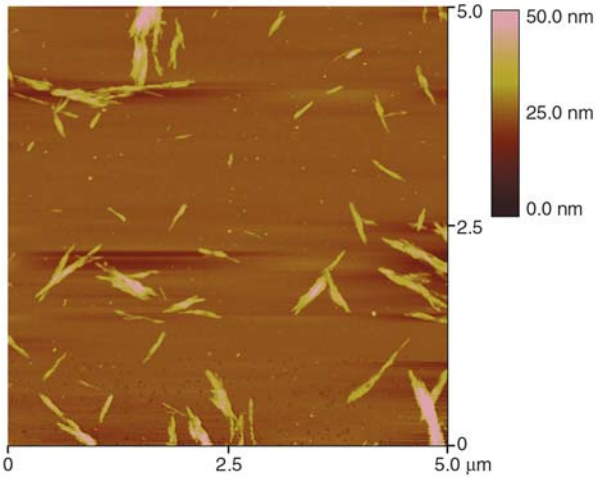

Figure 1. AFM topography image of FCNs after drying on a mica surface

size, which have lengths (*L*) ranging from 100 to 500 nm and diameters (*D*) ranging from 10 to 30 nm.

Figure 2 shows the SEM images of the failure surfaces of PS matrix and nanocomposite films. As compared to the PS film, the morphology of the FCNs in the PS matrix can be easily identified. The FCNs appear as white dots, whose concentration on the failure surface of the nanocomposites is a direct function of the filler loading from 10 to 30 wt%. These white dots correspond to the nanocrystals in the perpendicular plane of the nanocomposite films. No large aggregates and a homogeneous distribution of the FCNs in the PS matrix were observed in all nanocomposite films, implying good adhesion between fillers and matrix. This is attributed to the good compatibility resulting from the chemical similarities between starch and cellulose and the hydrogen bonding interactions existing in the interface between fillers and matrix. Such an even and uniform distribution of the fillers in the matrix could play an important role in improving the mechanical performance of the resulting nanocomposite films as discussed later.

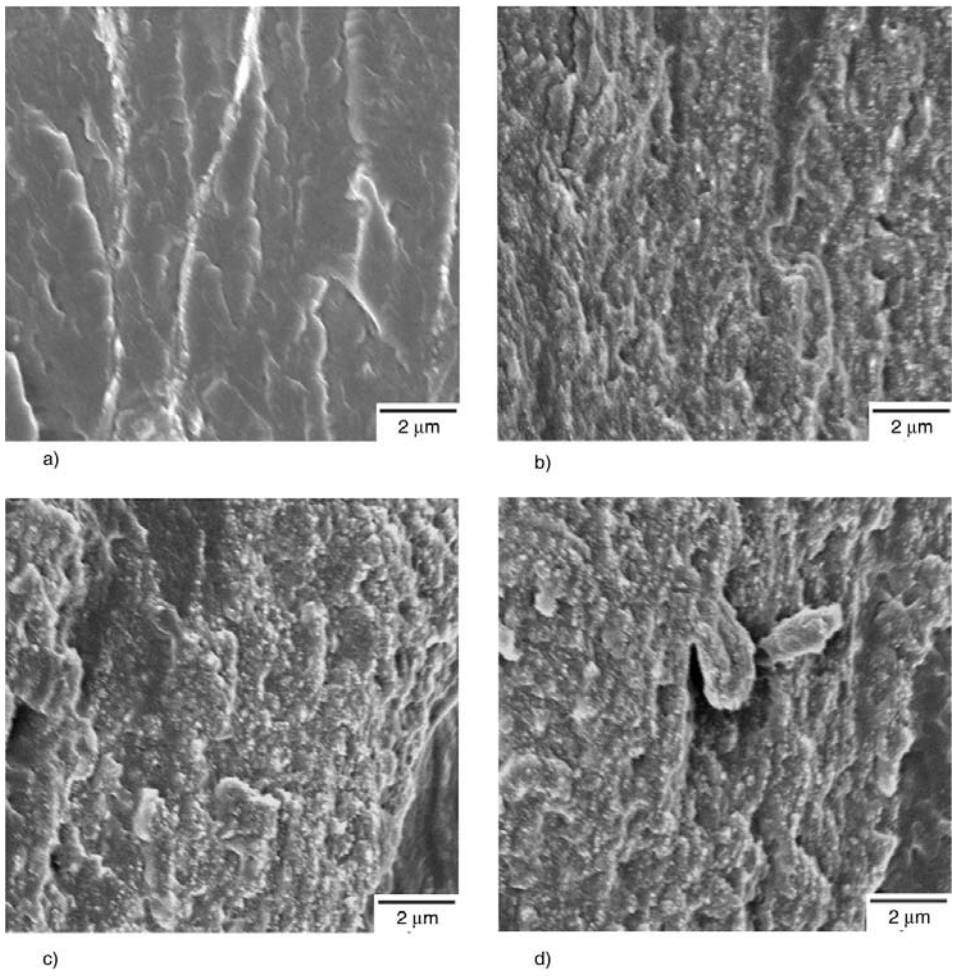

Figure 2. FESEM images of the failure surfaces of the PS and PS/FCNs nanocomposits with different FCNs content: a, 0 wt%; b, 10 wt%; c, 20 wt%; d, 30 wt%. (Scale bar: 2.0 µm)

3.2. Structure of PS/FCNs nanocomposites

Figure 3 shows the FTIR spectra of the PS, PS/FCNs-10, PS/FCNs-20 and PS/FCNs-30 films. The peaks at 3280 and 993 cm^{-1} in the spectra of PS were attributed to the stretching vibrations of the hydrogen bonding –OH groups and C–O stretching vibrations in starch, respectively [9, 28]. The composite films containing cellulose nanocrystals as filler exhibited almost the same FTIR spectra as the PS film due to the chemical similarities between starch and cellulose. However, the relative peak strength of stretching vibrations for –OH groups in the FTIR spectra composite films weakened, indicating the hydrogen bonding between starch molecules was partially destroyed. Furthermore, the wavenumber of the peak for C–O stretching vibrations shifted from 993 to 982 as FCNs content changed from 0 to 30 wt%, this suggested that new interactions between cellulose and starch molecules as a result of the addition of cellulose nanocrystals into starch.

The WAXD of the nanocomposites was studied as a function of the FCNs content and the corresponding diffractograms are shown in Figure 4. For the PS film, a typical C-type crystallinity pattern with peaks at $2\theta = 5.6°$ (characteristic of B type polymorphs), 17.0° (characteristic of both A and B type polymorphs), 20.1 and 22.5° (characteristic of B type polymorphs) were clearly observed [29]. The crystalline structure resulting from spontaneous recrystallization or retrogradation of starch molecules after melting or gelatinization has frequently been detected in food and thermoplastic materials

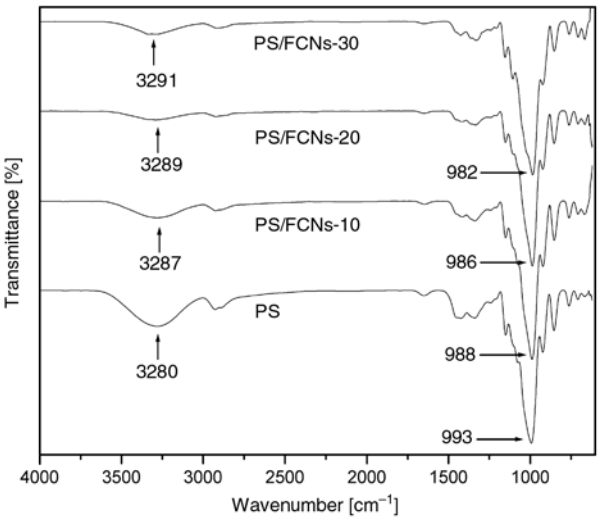

Figure 3. The FTIR spectra of the PS and PS/FCNs nanocomposite films

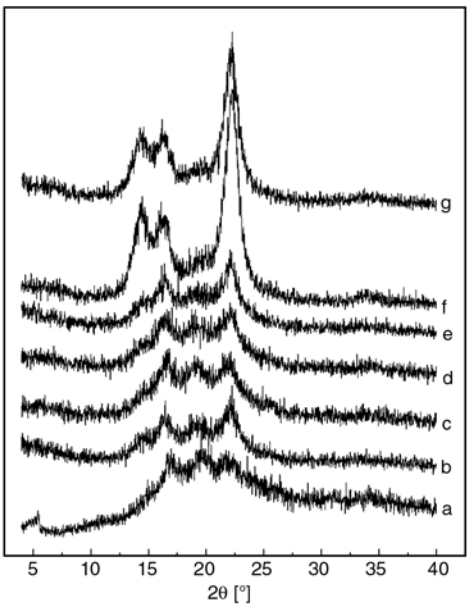

Figure 4. The WXRD patterns for PS and PS/FCNs nanocomposites: a – PS; b, PS/FCNs-5; c – PS/FCNs-10; d – PS/FCNs-15; e – PS/FCNs-20; f – PS/FCNs-25; g – PS/FCNs-30

[30]. In this case, the samples had been stored for more than 3 months before WAXD testing. With the addition of FCNs in the starch matrix, some diffraction peaks appear in the diffractograms. With an increase of the FCNs content in the films, the peaks become more significant. When the FCNs content increases to more than 20 wt%, three well-defined peaks at $2\theta = 14.7$, 16.5, and 22.7° are observed, which corresponds to the typical crystal pattern of cellulose I. Although the diffraction peak intensity of starch and cellulose in the nanocomposite changes with the composition ratio, no evidence of any additional peak or peak shift in the diffraction angles is observed. Therefore, it can be concluded that the diffractograms of nanocomposites are only superimpositions of the diffractograms of the two components.

3.3. Thermal analysis

Figure 5 shows the DSC thermograms in the temperature range of –100 to 120°C of the PS/FCNs nanocomposites conditioned at 43% *RH*. As we know, in DSC experiments, the glass transition temperature (T_g) is generally taken as the inflection point of the specific heat increment at the glass-rubber transition. From Figure 5 it is obvious that all samples display two distinct specific heat increments, which correspond to the glass transitions of

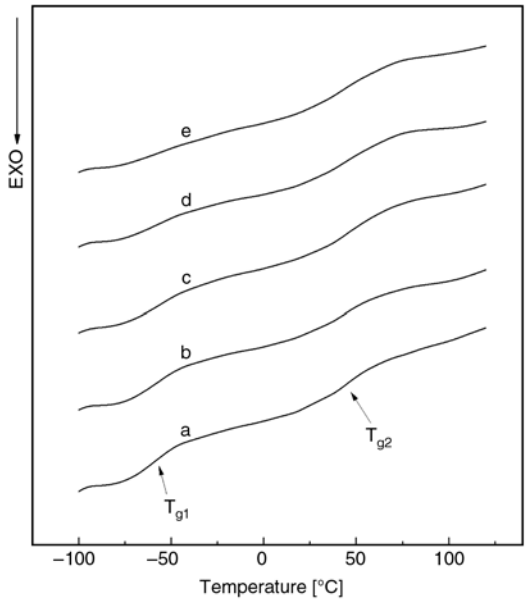

Figure 5. DSC thermograms of PS and PS/FCNs nanocomposites with different FCNs content: a – 0 wt%; b – 5 wt%; c – 10 wt%; d – 20 wt%; e – 30 wt%

the PS matrix. The values of T_g for all the nanocomposites are tabulated in Table 1. As Dufresne et al have previously reported, the PS plasticized by glycerol is a complex heterogeneous system composed of glycerol-rich domains dispersed in a starch-rich continuous phase and each phase exhibits its own T_g [31]. Therefore, the transitions located in the temperature ranged from –80 to –50°C and from 30 to 60°C can be assigned to T_{g1} of glycerol-rich phase and T_{g2} starch-rich phase respectively. With an increase in the FCNs fillers from 0 to 30 wt%, no obvious change of the value of T_{g1} at low temperature for the glycerol-rich phase is observed. However, T_{g2} for starch-rich phase shifts to higher temperature from 43.3 to 48.8°C, which indicates that FCNs restrict the mobility of starch chains due to the strong intermolecular interactions between starch and stiff FCNs.

3.4. Mechanical properties

The mechanical properties of the neat PS matrix films as well as the nanocomposite films reinforced with various contents of FCNs were investigated by tensile testing at room temperature. The typical stress-strain curves of the PS and its FCNs nanocomposites are shown in Figure 6. Generally, the nanocomposite films exhibit two characteristic regions of deformation behaviour. At low strains (<10%), the stress increases rapidly with an increase in strain. At higher strain the stress regularly increases with the strain increasing up to the break of the films. No evidence of necking phenomenon at the stress-strain curves confirms the good dispersion of the FCNs in the matrix and homogeneous morphology of the nanocomposites, which correlates with the results from SEM images. The dependence of tensile strength, Young's modulus, and elongation at break on FCNs content for the PS/FCNs nanocomposites is plotted in Figure 7, and the corresponding data are presented in Table 2. From the results we can see that the FCNs content has a profound effect on the mechanical properties. The tensile strength increases from 3.9 to 11.9 MPa and Young's modulus increase signifi-

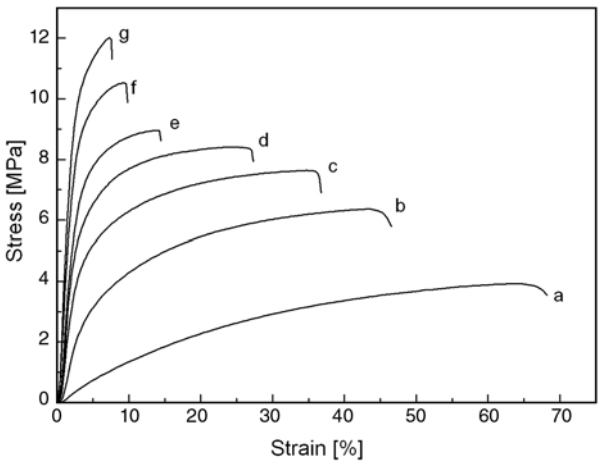

Figure 6. Stress-strain curves of PS and PS/FCNs nanocomposite films with FCNs content: a – 0 wt%; b – 5 wt%; c – 10 wt%; d – 15 wt%; e – 20 wt%, f – 25 wt%; g – 30 wt%

Table 1. The DSC data of PS and the PS/FCNs nanocomposites

Sample	$T_{g1,\,mid}$ [°C]	ΔCp [J/g·K]	$T_{g2,\,mid}$ [°C]	ΔC_p [J/g·K]
PS	–58.3	0.375	43.3	0.419
PS/FCNs-5	–55.8	0.319	44.9	0.550
PS/FCNs-10	–56.7	0.321	47.2	0.613
PS/FCNs-20	–55.1	0.319	47.8	0.497
PS/FCNs-30	–55.6	0.247	48.8	0.619

Table 2. Mechanical properties of PS and PS/FCNs nanocomposites obtained from tensile tests: tensile strength (σ), Young's modulus (*E*), and elongation at break (ε_B)

Sample	σ [MPa]	E [MPa]	ε_B [%]
PS	3.9 ± 0.3	31.9 ± 5.1	68.2 ± 3.1
PS/FCNs-5	6.4 ± 0.2	82.6 ± 5.3	44.3 ± 5.2
PS/FCNs-10	7.6 ± 0.3	180.4 ± 13.2	35.9 ± 4.3
PS/FCNs-15	8.2 ± 0.4	255.3 ± 12.1	26.8 ± 5.5
PS/FCNs-20	8.9 ± 0.3	311.9 ± 20.5	14.1 ± 4.2
PS/FCNs-25	10.5 ± 0.5	447.5 ± 14.3	9.4 ± 1.6
PS/FCNs-30	11.9 ± 0.8	498.2 ± 23.4	7.2 ± 1.8

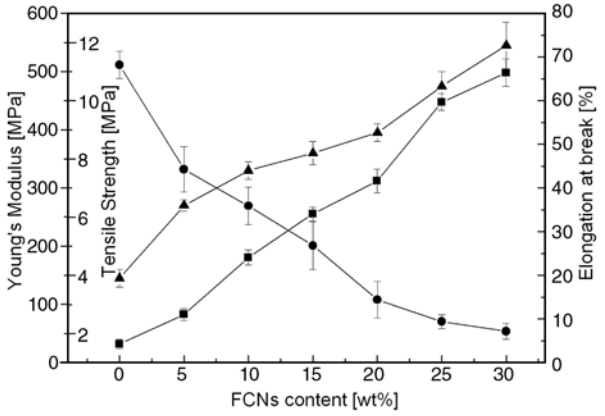

Figure 7. The mechanical properties of tensile strength (▲), Young's modulus (■), and elongation at break (●) of PS/FCNs nanocomposite as a function of FCNs content

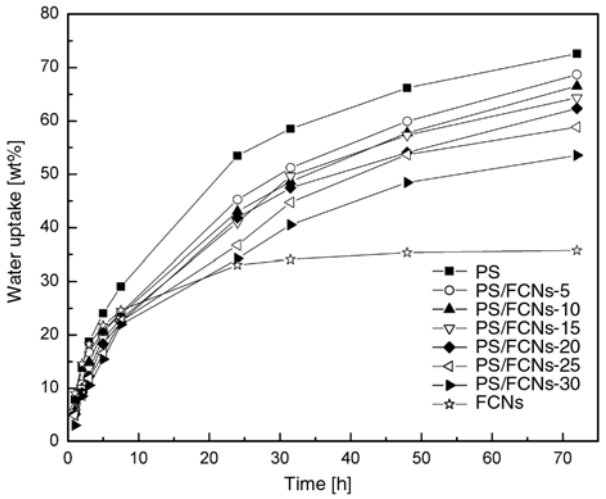

Figure 8. Water uptake during conditioning in 98% *RH* as a function of time for the PS and PS/FCNs films

cantly from 31.9 to 498.2 MPa with increasing filler content from 0 to 30 wt%, respectively, while the elongation at break decreases from 68.2 to 7.2%. This can probably be explained by the reinforcement effect from the homogeneously dispersed high-performance FCNs fillers in the PS matrix and the strong hydrogen bonding interaction between FCNs and PS molecules. The cellulose nanocrystals from flax fiber showed an effect similar to that of ramie-based [32] on the mechanical properties in the PS-based nanocomposites.

3.5. Water sensitivity

The water uptake of the PS and PS/FCNs films during conditioning in 98% *RH* as a function of time is shown in Figure 8. After 72 h, the water uptake of the PS film and FCNs is around 70 and 35 wt%, respectively. After incorporating FCNs into the PS matrix, the water uptake decreased as the FCNs content increased, and it was about 50 wt% for the PS/FCNs-30. Therefore, it can be concluded that the swelling of the material is suppressed in the presence of FCNs within the PS matrix. This phenomenon can be ascribed firstly to the low water uptake of the FCNs itself; and secondly to the presence of strong hydrogen bonding interactions between filler/filler and filler/matrix. Meanwhile, the low glycerol content to the whole material might also be responsible for the reduction of the water uptake.

4. Conclusions

A suspension of cellulose nanocrystals was prepared from flax fibers by acid hydrolysis and used to reinforce the PS matrix with content from 5 to 30 wt% for preparation of nanocomposite materials by a casting method. The SEM images showed that the FCNs fillers dispersed well within the PS matrix and had good adhesion in the interfacial area. The values of T_g ascribed to the starch-rich phase increased with increasing content of FCNs, indicating that the existence of FCNs reduced the flexibility of starch molecular chains. It is worth noting that the tensile strength and Young's modu-

lus of the nanocomposites increased, respectively, from 3.9 to 11.9 MPa and from 31.9 to 498.2 MPa with an increase of FCNs content from 0 to 30 wt%. Meanwhile, the starch-based nanocomposites also show a higher water resistance. The performance improvements of the PS/FCNs nanocomposites may be ascribed to the chemical similarities between starch and cellulose and the hydrogen bonding interactions existing in filler/matrix.

Acknowledgements

This work was financially supported in part by the Agricultural Bioproducts Innovation Program (ABIP) of Canada via Pulse Research Network (PURENET) and Next Generation BioProducts for Health and Wellness Network (NGBHW).

References

[1] Yu L., Dean K., Li L.: Polymer blends and composites from renewable resources. Progress in Polymer Science, **31**, 576–602 (2006).

[2] de Menezes A. J., Pasquini D., Curvelo A. A. S., Gandini A.: Novel thermoplastic materials based on the outer-shell oxypropylation of corn starch granules. Biomacromolecules, **8**, 2047–2050 (2007).

[3] Mohanty A. K., Misra M., Hinrichsen G.: Biofibres, biodegradable polymers and biocomposites: An overview. Macromolecular Materials and Engineering, **276–277**, 1–24 (2000).

[4] Mathew A. P., Dufresne A.: Morphological investigation of nanocomposites from sorbitol plasticized starch and tunicin whiskers. Biomacromolecules, **3**, 609–617 (2002).

[5] Tábi T., Kovács J. G.: Examination of injection moulded thermoplastic maize starch. Express Polymer Letters, **1**, 804–809 (2007).

[6] Santayanon R., Wootthikanokkhan J.: Modification of cassava starch by using propionic anhydride and properties of the starch-blended polyester polyurethane. Carbohydrate Polymers, **51**, 17–24 (2003).

[7] Cao X., Chang P. R., Huneault M. A.: Preparation and properties of plasticized starch modified with poly(ε-caprolactone) based waterborne polyurethane. Carbohydrate Polymers, **71**, 119–125 (2008).

[8] Cao X., Zhang L., Huang J., Yang G., Wang Y.: Structure-properties relationship of starch/waterborne polyurethane composites. Journal of Applied Polymer Science, **90**, 3325–3332 (2003).

[9] Chen Y., Cao X., Chang P. R., Huneault M. A.: Comparative study on the films of poly(vinyl alcohol)/pea starch nanocrystals and poly(vinyl alcohol)/native pea starch. Carbohydrate Polymers, **73**, 8–17 (2008).

[10] Cao X., Zhang L.: Miscibility and properties of polyurethane/benzyl starch semi-interpenetrating polymer networks. Journal of Polymer Science, Part B: Polymer Physics, **43**, 603–615 (2005).

[11] Cao X., Zhang L.: Effects of molecular weight on the miscibility and properties of polyurethane/benzyl starch semi-interpenetrating polymer networks. Biomacromolecules, **6**, 671–677 (2005).

[12] Cao X., Wang Y., Zhang L.: Effects of ethyl and benzyl groups on the miscibility and properties of castor oil-based polyurethane/starch derivative semi-interpenetrating polymer networks. Macromolecular Bioscience, **5**, 863–871 (2005).

[13] Suda K., Kanlaya M., Manit S.: Synthesis and property characterization of cassava starch grafted poly[acrylamide-co-(maleic acid)] superabsorbent via γ-irradiation. Polymer, **43**, 3915–3924 (2002).

[14] Lepifre S., Froment M., Cazaux F., Houot S., Lourdin D., Coqueret X., Lapierre C., Baumberger S.: Lignin incorporation combined with electron-beam irradiation improves the surface water resistance of starch films. Biomacromolecules, **5**, 1678–1686 (2004).

[15] Chen B., Evans J. R. G.: Thermoplastic starch-clay nanocomposites and their characteristics. Carbohydrate Polymers, **61**, 455–463 (2005).

[16] Cao X., Chen Y., Chang P. R., Huneault M. A.: Preparation and properties of plasticized starch/multiwalled carbon nanotubes composites. Journal of Applied Polymer Science, **106**, 1431–1437 (2007).

[17] Šturcová A., Davies G. R., Eichhorn S. J.: Elastic modulus and stress-transfer properties of tunicate cellulose whiskers. Biomacromolecules, **6**, 1055–1061 (2005).

[18] Azizi Samir M. A. S., Alloin F., Dufresne A.: Review of recent research into cellulosic whiskers, their properties and their application in nanocomposite field. Biomacromolecules, **6**, 612–626 (2005).

[19] Dubief D., Samain E., Dufresne A.: Polysaccharide microcrystals reinforced amorphous poly(β-hydroxyoctanoate) nanocomposite materials. Macromolecules, **32**, 5765–5771 (1999).

[20] Wang Y., Cao X., Zhang L.: Effects of cellulose whiskers on properties of soy protein thermoplastics. Macromolecular Bioscience, **6**, 524–531 (2006).

[21] Noshiki Y., Nishiyama Y., Wada M., Kuga S., Magoshi J.: Mechanical properties of silk fibroin-microcrystalline cellulose composite films. Journal of Applied Polymer Science, **86**, 3425–3429 (2002).

[22] Helbert W., Cavaille J. Y., Dufresne A.: Thermoplastic nanocomposites filled with wheat straw cellulose whiskers. Part I: Processing and mechanical behavior. Polymer Composites, **17**, 604–611 (1996).

[23] Chazeau L., Cavaillé J. Y., Canova G., Dendievel R., Boutherin B.: Viscoelastic properties of plasticized PVC reinforced with cellulose whiskers. Journal of Applied Polymer Science, Part B: Polymer Physics, **71**, 1797–1808 (1999).

[24] Ljungberg N., Bonini C., Bortolussi F., Boisson C., Heux L., Cavaille J. Y.: New nanocomposite materials reinforced with cellulose whiskers in atactic polypropylene: Effect of surface and dispersion characteristics. Biomacromolecules, **6**, 2732–2739 (2005).

[25] Cao X., Dong H., Li C. M.: New nanocomposite materials reinforced with flax cellulose nanocrystals in waterborne polyurethane. Biomacromolecules, **8**, 899–904 (2007).

[26] Smeder B., Liljedahl S.: Market oriented identification of important properties in developing flax fibres for technical uses. Industrial Crops and Products, **5**, 149–162 (1996).

[27] Dong X. M., Kimura T., Revol J-F., Gray D. G.: Effects of ionic strength on the isotropic-chiral nematic phase transition of suspensions of cellulose crystallites. Langmuir, **12**, 2076–2082 (1996).

[28] Zhang Y., Han J. H.: Plasticization of pea starch gilms with monosaccharides and polyols. Journal of Food Science, **71**, E253–E261 (2006).

[29] Rindlava A., Hulleman S. H. D., Gatenholma P.: Formation of starch films with varying crystallinity. Carbohydrate Polymers, **34**, 25–30 (1997).

[30] Souza Rosa R. C. R., Andrade C. T.: Effect of chitin addition on injection-molded thermoplastic corn starch. Journal of Applied Polymer Science, **92**, 2706–2713 (2004).

[31] Angles M. N., Dufresne A.: Plasticized starch/tunicin whiskers nanocomposites. 1. structural analysis. Macromolecules, **33**, 8344–8353 (2000).

[32] Lu Y., Weng L., Cao X.: Morphological, thermal and mechanical properties of ramie crystallites-Reinforced plasticized starch biocomposites. Carbohydrate Polymers, **63**, 198–204 (2006).